Journal of Nuclear Materials 172 (1990) 54–70
North-Holland

ANALYSIS OF SINGULAR STRESS FIELDS IN DUPLEX FUSION COMPONENTS

James P. BLANCHARD

Department of Nuclear Engineering and Engineering Physics, University of Wisconsin – Madison, 1500 Johnson Drive, Madison, WI 53706, USA

Nasr M. GHONIEM

Mechanical, Aerospace, and Nuclear Engineering Department, University of California – Los Angeles, Los Angeles, CA 90024, USA

Received 25 September 1989; accepted 2 February 1990

Thermal and swelling stress fields in bonded structures are sought using a model consisting of two thin, rectangular strips perfectly bonded along one surface. Existing results for stresses in the bulk, based on beam theory, are presented and their limitations are discussed. Plane elasticity is used to derive general solutions for the stress fields near the edge of the structure, in many cases yielding logarithmic or algebraic singularities. Methods for coupling these general edge fields to the stresses in the bulk are discussed, and the techniques are applied to materials and loading conditions relevant to fusion components. The impact of swelling and creep on both the order of the singularity and on its intensity is shown.

1. Introduction

Layered structures are characteristic of many components in both near-term and commercial fusion machines. Limiters, divertors, and first walls must be able to withstand increasing particle and heat fluxes without failure and without degrading the plasma, while maintaining reasonable peak temperatures. These concerns have led many designers to employ duplex structures to allow the use of different materials, thus satisfying the often conflicting requirements of low sputtering rate and high strength. These structures typically use either a low-Z or very low sputtering plasma-facing material (graphite and tungsten are common), bonded to a metal substrate (typically copper, steel, or Incaloy). The bonding of these layers leads to complicated stress fields which must be understood in order to evaluate the probability of failure for the device.

Thermal and swelling stresses in bonded structures arise from two sources. The first is the self-constraint of differential expansion, caused by differing thermal expansion coefficients or differential swelling. The second source of stress is the self-constraint of thermal or swelling gradients, which can occur both in bonded and single-material components. In either case, the stress in the bulk of the component is generally a uniform, uniaxial stress field consisting only of axial stresses which vary over the thickness. Only near the ends of the strips, where edge effects must be considered, are the stress fields multiaxial. These edge fields, though they typically make up only a small part of the total component volume, are significant because bond failure often begins where an interface intersects a free surface, i.e. at the end of the strips. Hence, this paper will calculate the edge stress fields in a variety of idealized fusion components.

Stresses in the bulk of bonded structures can be analyzed using beam theory, giving stress fields that depend only on the distance from the neutral axis of the composite. This has been done previously for many applications other than fusion, so this paper will merely present a summary of the typical stress fields found in bonded strips. The solutions based on beam theory (assuming that plane sections remain plane) are valid only at points which are sufficiently removed from the ends of the beam, so a more detailed two-dimensional analysis is needed if one wants to capture the stresses near the edge of the interface. Elastic solutions for edge fields in bonded structures yield singularities at the edge of the interface, thus violating the small strain assumptions of the linearized elasticity equations. These singularities complicate the analysis of bonded structures,

making such convenient techniques as finite element methods very difficult. One technique for dealing with these singularities will be presented here for fusion reactor applications.

This paper presents an overview of the various types of stress singularities found in bonded structures. It begins with a brief discussion of stresses in the bulk of such structures, then follows with a treatment of singularities at the edge. The final section considers applications to fusion, including stresses induced by swelling and relaxed by irradiation creep.

2. Analysis of bulk stresses in bonded structures

In this section, solutions for the bulk stresses in two laminated strips are given, drawing from previous work by Timoshenko [1]. Additional discussion of the topic can be found in Boley and Weiner [2]. The model used for this analysis, shown in fig. 1, consists of two perfectly bonded strips of different materials. The properties of the top strip are denoted by a double prime (i.e., E'', ν'', and α''), while those of the lower strip are denoted by a single prime (E', ν', and α'). There are no imperfections in this model, and there is no constraint of bending of the composite.

A critical outcome of the analysis is the curvature of the composite. For a uniform temperature change from the undeformed configuration, Timoshenko finds the final curvature to be:

$$\frac{1}{\rho} = \frac{6(\alpha' - \alpha'')T(1+\xi)^2}{(t'+t'')\left[3(1+\xi)^2 + (1+\xi\eta)\left(\xi^2 + 1/\xi\eta\right)\right]}, \tag{1}$$

where ρ is the radius of curvature of the composite, t is the strip thickness, α is the thermal expansion coefficient, T is the temperature change (positive for an increase form the undeformed configurations), and ξ and η are given by:

$$\xi = t''/t' \tag{2}$$

and

$$\eta = E''/E'. \tag{3}$$

The maximum stress in the composite (ignoring stress fields near the edge), which occurs at the interface, is given by:

$$\sigma_{\max} = \frac{1}{\rho}\left[\frac{2(E''I'' + E'I')}{t''(t''+t')} + \tfrac{1}{2}E''t''\right], \tag{4}$$

where I is the moment of inertia of the individual strips (i.e., $I = t^3/12$).

Two simplified cases provide examples of the relative importance of the material properties to the stresses in duplex structures. If the two strips are of equal thickness ($t' = t'' = t$), then the curvature is given by:

$$\frac{1}{\rho} = \frac{12\eta(\alpha' - \alpha'')T}{t(\eta^2 + 14\eta + 1)}, \tag{5}$$

and the peak stress is given by:

$$\sigma_{\max} = \frac{\eta(1+7\eta)}{\eta^2 + 14\eta + 1}E'(\alpha' - \alpha'')T. \tag{6}$$

It is obvious that the peak stresses in the bulk of bonded strips are proportional to the difference in the thermal expansion coefficients, but it is perhaps less obvious that the deformations are only weakly dependent on the ratio of the moduli of the two materials. Timoshenko shows that doubling (or halving) the ratio of the elastic moduli of the two materials leads to only a 3% difference in the curvature of the composite.

As will be seen later in this paper, the simplicity of the above analysis is misleading. Rigorous, two-dimensional analysis of the edge fields in bonded structures yields complicated stress fields which require extensive analysis for an accurate determination. It is tempting to argue that the edges constitute only a small part of a typically thin bonded component, but the propensity of such devices to fail near the edge (by debonding or cracking) makes this small region critical. The following section discusses the types of stress fields that one might encounter in performing an elastic analysis in the vicinity of the intersection between an interface and a free surface.

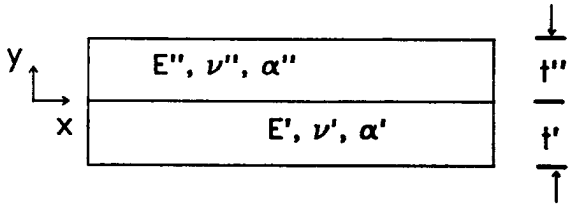

Fig. 1. Model for analysis of stresses in two-dimensional duplex structures.

3. Stress singularities at interface edges

The shortfall of the beam theory approach presented in the previous section is the absence of any analysis of

edge effects. Beam theories assume that plane sections remain plane as the structure deforms, but this breaks down at the ends of the beam due to the presence of the free surface. Hence, the beam theory breaks down at distances less than the order of the beam thickness from the end (according to Saint-Venant's Principle) and more detailed modeling is required to accurately capture the stress fields near the edge. In general these stress fields feature substantial contributions from all three relevant stress components (σ_{xx}, σ_{yy}, and σ_{xy}), as opposed to the 1-D field (σ_{xx}) encountered in the bulk of the bonded strips. An additional complication of these edge fields arises from the tendency of the stresses to be singular at the point where the interface intersects a free surface.

Typically, the stresses along the interface of two bonded strips (such as the model shown in fig. 1) can be divided into two regions: a bulk region consisting of all the material a sufficient distance from the edges and two edge regions. In the bulk of the strips, the shear and normal stresses (σ_{xy} and σ_{yy}) are essentially zero, while the axial stress (σ_{xx}) is non-zero and can be calculated with simple beam theory. Near the edge, though, all three stresses are non-zero, indicating the existence of a boundary layer near the free surfaces. According to Williams [3], the thickness of this layer is of the order $\sqrt{tL}$, where t is the model thickness and L is the model length. These edge fields can be represented reasonably well using a variational approach (see, for instance, refs. [3–5]), but these techniques require extremely complicated algebraic manipulation for even the simplest loadings and geometries and they are not useful for edge singularities, which are of particular interest for this study. Hence, other techniques are needed for studying edge fields in bonded structures.

This section, then, deals with the nature of edge stresses in perfectly bonded strips. No cracks, slippage, or debonding will be considered. In this sense, the analysis presented here represents a study of the initiation of failure at the edge of the interface of a laminated structure. In bodies (either single- or multi-layered) containing cracks, linear elastic fracture mechanics predicts a stress field of the form

$$\sigma_{ij} \sim \frac{K}{\sqrt{r}} \quad \text{for} \quad r \to 0 \tag{7}$$

at the tip of the crack, where r is the distance from the crack tip. The stress intensity factor K is considered to be a measure of the intensity of the stress singularity, and has been shown to be a useful predictor of crack growth. As will be shown in the following section, the

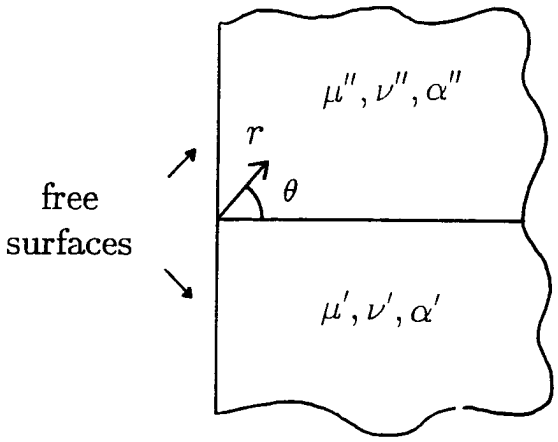

Fig. 2. Model for semi-infinite quarter planes to determine stresses at the edge of the interface.

stress field in a crack-free, bonded structure is generally of the form:

$$\sigma_{ij} \sim \frac{K}{r^{\delta}} \quad \text{for} \quad r \to 0, \tag{8}$$

where $0 \le \delta \le 0.41$ for structures composed of bonded rectangles. (The order of the singularity depends both on geometry and material properties.) Therefore, crack-free, bonded components exhibit a relatively weak singularity analogous to that for the stress field near a crack tip. This paper assumes that the initiation of failure in bonded structures can be predicted by the "stress intensity" associated with the edge of a perfect interface, making knowledge of the characteristics of such stress fields vital to the design of bonded structures. This assumption, of course, requires experimental verification.

The stresses at the edge of the interface between two materials can be sought by considering bonded semi-infinite quarter-planes. The model used for this purpose is shown in fig. 2. Using the Airy stress function, one can determine a stress field that satisfies the field equations in the bulk, the interface conditions, and the traction conditions on the free surfaces adjacent to the interface. This yields an infinite series with undetermined coefficients, which can be determined by considering the finite extent of the original model shown in fig. 1. An outline of the procedures required for this analysis follows: details can be found in a recent paper by the authors [6].

The analysis begins with the two-dimensional, steady-state, elastic field equations in polar coordinates (assuming no body forces are present), along with the

traction-free boundary conditions and the assumed interface conditions:

strain–displacement:

$$\epsilon_{rr} = u_{r,r}, \tag{9}$$

$$\epsilon_{\theta\theta} = \frac{u_r}{r} + \frac{u_{\theta,\theta}}{r}, \tag{10}$$

$$\epsilon_{r\theta} = \frac{1}{2}\left(\frac{1}{r}u_{r,\theta} + u_{\theta,r} - \frac{u_\theta}{r}\right); \tag{11}$$

stress–strain:

$$\sigma_{rr} = 2\mu\epsilon_{rr} + \lambda\epsilon_{II} - (2\mu + 3\lambda)\epsilon_{\text{in}}, \tag{12}$$

$$\sigma_{\theta\theta} = 2\mu\epsilon_{\theta\theta} + \lambda\epsilon_{II} - (2\mu + 3\lambda)\epsilon_{\text{in}}, \tag{13}$$

$$\sigma_{r\theta} = 2\mu\epsilon_{r\theta}; \tag{14}$$

equilibrium:

$$\sigma_{rr,r} + \frac{\sigma_{r,\theta\theta}}{r} + \frac{\sigma_{rr} - \theta_{r\theta}}{r} = 0, \tag{15}$$

$$\frac{\sigma_{\theta\theta,\theta}}{r} + \sigma_{r\theta,r} + 2\frac{\sigma_{r\theta}}{r} = 0; \tag{16}$$

boundary conditions:

$(\theta = \pm\pi/2)$,

$$\sigma_{\theta\theta} = \sigma_{r\theta} = 0; \tag{17}$$

interface conditions:

$(\theta = 0)$,

$$\sigma'_{\theta\theta} = \sigma''_{\theta\theta}, \tag{18}$$

$$\sigma'_{r\theta} = \sigma''_{r\theta}, \tag{19}$$

$$u'_r = u''_r, \tag{20}$$

$$u'_\theta = u''_\theta. \tag{21}$$

In these equations, σ_{ij} represents a stress, ϵ_{ij} represents a strain, u_r and u_θ represent the radial and azimuthal deflections, respectively, and λ and μ are the Lamé material constants. The inelastic strain ϵ_{in} is the sum of the thermal and swelling strains, each representing an isotropic volume change, i.e.

$$\epsilon_{\text{in}} = \alpha T + \Delta V/3V, \tag{22}$$

where α is the thermal expansion coefficient, T is the difference between the temperature in the component and some zero-stress reference temperature, and $\Delta V/3V$ is the swelling strain. Also σ'_{ij} denotes a stress in the lower of the two strips, while σ''_{ij} denotes stress in the upper strip. A similar notation will be used for displacements and material properties as well.

In order to reduce the problem to determination of a scalar function, the Airy stress function Φ is introduced according to the standard definition:

$$\sigma_{rr} = \frac{1}{r}\Phi_{,r} + \frac{1}{r^2}\Phi_{,\theta\theta}, \tag{23}$$

$$\sigma_{\theta\theta} = \Phi_{,rr}, \tag{24}$$

$$\sigma_{r\theta} = \frac{1}{r^2}\Phi_{,\theta} - \frac{1}{r}\Phi_{,r\theta}. \tag{25}$$

Stress fields determined from a stress function of this type automatically satisfy the equilibrium equations.

If the displacements u_r and u_θ, determined from a known stress field, are to be single-valued, then the stresses must satisfy the compatibility equation:

$$\nabla^2(\sigma_{rr} + \sigma_{\theta\theta}) + QE\nabla^2\epsilon_{\text{in}} = 0, \tag{26}$$

where Q is given by

$$Q = \begin{cases} 1 & \text{for plane stress,} \\ 1/(1-\nu) & \text{for plane strain.} \end{cases} \tag{27}$$

Finally, in terms of the stress function, the displacements are given by:

$$u_{r,r} = \frac{1}{2\mu}\left[\frac{1}{r}\Phi_{,r} + \frac{1}{r^2}\Phi_{,\theta\theta} - \left(1 - \frac{m}{4}\right)\nabla^2\Phi\right] + n\epsilon_{\text{in}} \tag{28}$$

and

$$u_{\theta,r} - \frac{u_\theta}{r} + \frac{1}{r}u_{r,\theta} = \frac{1}{\mu}\left(\frac{1}{r^2}\Phi_{,\theta} - \frac{1}{r}\Phi_{,r\theta}\right), \tag{29}$$

where

$$m = \begin{cases} 4/(1+\nu) & \text{for plane stress,} \\ 4(1-\nu) & \text{for plane strain,} \end{cases} \tag{30}$$

and

$$n = \begin{cases} 1 & \text{for plane stress,} \\ (1+\nu) & \text{for plane strain.} \end{cases} \tag{31}$$

Inserting eqs. (23) and (24) into the compatibility equation yields the following fourth order partial differential equation for the stress function (again assuming no body forces):

$$\nabla^4\Phi + QE\nabla^2\epsilon_{\text{in}} = 0. \tag{32}$$

Solving for the stress function, subject to the appropriate surface traction and interface conditions, provides a means for computing the steady-state stresses, strains, and displacements in a planar medium.

In this study, the thermal and swelling fields are harmonic (satisfying Fourier's Law of conduction for a body in a steady-state) and the swelling strains are assumed to be uniform. The assumption of linear thermal fields is generally valid, but the swelling may not be uniform for three reasons:

1. Gradients in the damage rate, due to flux attenuation, can lead to swelling gradients. This is a small effect in the thin structures generally found in high heat-flux fusion components.
2. The temperature dependence of the swelling rate can lead to swelling gradients in the presence of thermal gradients. No measurements of this effect have been conducted.

3. The stress dependence of swelling could lead to swelling gradients in the presence of stress gradients. Swelling is thought to be increased slightly by positive hydrostatic stresses.

These effects are all presumed to be small, but further testing is required to substantiate the uniform swelling assumption. Assuming that the inelastic strain fields are harmonic, the stress function is governed by:

$$\nabla^4 \Phi = 0. \tag{33}$$

In order to reduce this partial differential equation for the Airy stress function to an ordinary differential equation, the solution is assumed to be of the form:

$$\Phi = r^{-s} F(\theta). \tag{34}$$

Under this transformation the equation for the stress function (eq. (33)) becomes

$$\left(\frac{d^2}{d\theta^2} + s^2\right)\left(\frac{d^2}{d\theta^2} + (s+2)^2\right) F = 0. \tag{35}$$

Also, the stresses are given by:

$$\sigma_{rr} = \left(\frac{d^2}{d\theta^2} + s^2\right) F r^{-(s+2)}, \tag{36}$$

$$\sigma_{\theta\theta} = s(s+1) F r^{-(s+2)}, \tag{37}$$

and

$$\sigma_{r\theta} = (s+1)\frac{dF}{d\theta} r^{-(s+2)}. \tag{38}$$

For $s \neq 0$, -2 the general form of the stress function, from eq. (35) is:

$$F = a \sin s\theta + b \cos s\theta + c \sin(s+2)\theta + d \cos(s+2)\theta, \tag{39}$$

where a, b, c, and d are unknown constants.

Given a solution for the stress function in each quarter-plane of the model, the full solution is obtained by using the boundary and interface conditions to determine the four unknown constants in each strip. This leads to a system of eight linear equations, which can be written in the following form:

$$[X]\{a\} = \{f\}, \tag{40}$$

where $[X]$ is an 8×8 coefficient matrix depending on the Mellin parameter s and the material properties, $\{a\}$ is an 8 element vector of unknown constants, and $\{f\}$ is an 8 element forcing vector depending on the loadings. The solution of this system provides the stresses and displacements in bonded, semi-infinite quarter-planes.

The homogeneous solution of the problem is found by setting the forcing vector in eq. (40) to zero. A nontrivial solution to this equation only exists if the determinant of the matrix is zero. This leads to a characteristic equation of the form:

$$\| X \| = 0, \tag{41}$$

where $\| X \|$ is the determinant of the matrix in eq. 40 and is given by:

$$\| X \| = k_3^2 \eta^2 + \tfrac{1}{4} k_1^2 (\gamma\delta - \eta^2)^2 - k_2^2 \gamma\delta + \tfrac{1}{2} k_2 k_1 (\delta - \gamma)(\gamma\delta - \eta^2), \tag{42}$$

where η, γ, and δ are given by:

$$\eta = -2 \sin \xi \cos \xi, \tag{43}$$

$$\gamma = 2(s+1) - 2 \cos 2\xi, \tag{44}$$

$$\delta = 2(s+1) + 2 \cos 2\xi, \tag{45}$$

and k_1, k_2, and k_3 are material constants determined by:

$$k_1 = 2(k-1), \tag{46}$$

$$k_2 = km'' - m', \tag{47}$$

$$k_3 = km'' + m', \tag{48}$$

and

$$k = \mu'/\mu''. \tag{49}$$

The values of s corresponding to the roots of the determinant are discussed in the next section.

3.1. Roots of the determinant

Because the strain energy density is proportional to σ_{ij}^2, it will be proportional to $r^{-2(s+2)}$. Hence, for the total strain energy to be finite, s must be less than -1. Therefore, only roots of the determinant that have real parts less than -1 are admissible. In addition, roots that lie in the region $-2 < s < -1$ lead to singular stress fields, so they are of particular interest. For all k_1, k_2, and k_3 (i.e. for any combination of materials), $s = 0$, -1, and -2 are always zeroes. As has been demonstrated by the authors [6], the root at $s = -1$ provides rigid body translations, u_0 and v_0 and the root at $s = -2$ provides a rigid body rotation and, in certain cases [those for which $k_2(2k_1 - k_2) = 0$], a particular solution that must be used to form a solution for finite bodies.

Because the stresses are proportional to $r^{-(s+2)}$, they will be singular when there is a root on $-2 < s < -1$. It can be shown using eq. (42), that the parameter $P = k_2(2k_1 - k_2)$ determines the existence of roots on the interval $-2 < x < -1$. As it turns out, the parameter P is proportional to the derivative of the determinant of the matrix in eq. (40) at $s = -2$, so it is an indicator of

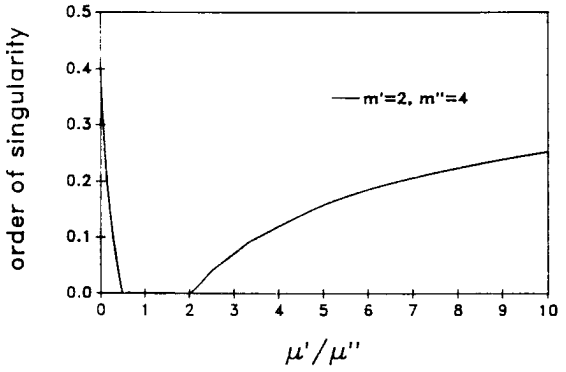

Fig. 3. Order of singularity for various material combinations.

the slope of the determinant at this point. For $P > 0$, there is exactly one zero on the interval $-2 < s < -1$, and it is a simple zero. For all admissible values of the material constants (i.e. $0 < \nu < \frac{1}{2}$), this zero occurs between -1.59 and -2.0. As P approaches zero, the zero of the determinant moves closer to $s = -2$ until, when $P = 0$, there are no zeroes on $-2 < s < -1$ and the zero at $s = -2$ becomes a double root. Finally, for $P > 0$, there are no zeroes on $-2 < s < -1$ and the zero at $s = -2$ is simple; also, there is a simple zero between -2.4 and -2.0.

As one might expect, singularities tend to occur when the elastic properties of the two materials differ significantly. This is shown in fig. 3, which shows the order of singularity as a function of the ratio of the shear moduli of the two layers for various values of m' and m''. The curves all peak at $k = 0$, which models a situation in which one material has zero shear stiffness. In this case, the singularity is of order 0.41, which is still smaller than the 0.5 associated with linear elastic fracture problems. As k increases, the order decreases until it reaches zero somewhere between $k = 0.5$ and $k = 0.9$. Above these transition values, the shear moduli of the two materials are closely matched ($k \to 1$) and the algebraic singularity disappears. The stresses then exhibit either a logarithmic singularity or the stresses are of order one.

The order of singularity is presented for a variety of material combinations in table 1. It is tempting to make judgements about the viability of certain material combinations using the results of this table, but one must avoid this trap for two reasons. First, the order of singularity does not depend on the thermal expansion coefficients, so the concept of good matching of this important property does not influence the values given in the table. This will be pursued further when the particular solutions are sought. The second factor not considered here is fabricability. Some material combinations form better bonds with each other, and this higher strength can lead to larger allowable loads. Experimental evidence is required to determine the importance of the order of the singularity in determining the propensity of a particular material combination to fail.

Table 1
Order of singularity at edge of interface

	Plane stress	Plane stress
Graphite/copper	0.065	0.069
Tungsten/copper	0.085	0.118
Graphite/vanadium	0.064	0.068
Tungsten/vanadium	0.089	0.124
Graphite/316 SS	0.084	0.092
Tungsten/316 SS	0.035	0.047

In order to determine the stresses in a finite bonded structure, all the roots of the determinant in eq. (42) must be determined. For certain material combinations (when k_2 is an even multiple of k_1) there are other integer roots, but the remaining roots are generally complex. A typical example of the spectrum of complex roots, determined numerically using Muller's method [7], is shown in fig. 4. Several observations can be made regarding these complex roots:

- they always appear as complex conjugates;
- for large negative real part, the real part of one root is about one unit from its neighbors;
- for increasing negative real part, the magnitude of the imaginary part increases much more slowly than the magnitude of the real part.

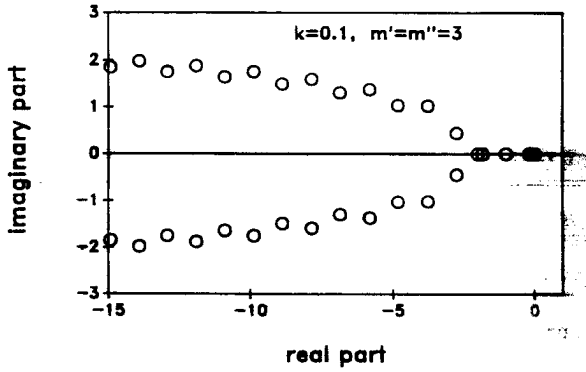

Fig. 4. Roots of determinant for $-15 \le s \le 0$. The number of roots is doubly infinite and the roots are symmetric about $\mathrm{Re}(s) = -1$.

These complex roots, combined with the real root on the interval $-2 < x < -1$ (if one exists), lead to a solution for the stresses and displacements in the form of an infinite series, represented by:

$$\sigma_{ij} = \sum_{k=1}^{\infty} a_k f_{ij(k)} r^{-(s_k+2)}, \tag{50}$$

$$u_r = \frac{1}{2\mu} \sum_{k=1}^{\infty} a_k f_{u_r(k)} r^{-(s_k+2)}, \tag{51}$$

$$u_\theta = \frac{1}{2\mu} \sum_{k=1}^{\infty} a_k f_{u_\theta(k)} r^{-(s_k+2)}, \tag{52}$$

where

$$\begin{aligned}
f_{rr(k)} &= [-A \sin s_k\theta - B \cos(s_k+2)\theta \\
&\quad -(s_k+4)C \sin(s_k+2)\theta \\
&\quad -(s_k+4)D \cos(s_k+2)\theta]s_k(s_k+1), \\
f_{r\theta(k)} &= [A \cos(s_k+2)\theta - B \sin(s_k+2)\theta \\
&\quad +(s_k+2)C \cos(s_k+2)\theta \\
&\quad -(s_k+2)D \sin(s_k+2)\theta]s_k(s_k+1), \\
f_{\theta\theta(k)} &= [A \sin(s_k+2)\theta + B \cos(s_k+2)\theta \\
&\quad +s_kC \sin(s_k+2)\theta + s_kD \cos(s_k+2)\theta] \\
&\quad \times s_k(s_k+1), \\
f_{u_r(k)} &= [A \sin(s_k+2)\theta + B \cos(s_k+2)\theta \\
&\quad +(s_k+m)C \sin(s_k+2)\theta \\
&\quad +(s_k+m)D \cos(s_k+2)\theta]s_k, \\
f_{u_\theta(k)} &= [A \cos(s_k+2)\theta - B \sin(s_k+2)\theta \\
&\quad +(s_k+2-m)C \cos(s_k+2)\theta \\
&\quad +(s_k+2-m)D \sin(s_k+2)\theta]
\end{aligned} \tag{53}$$

Because the complex roots s_k appear as complex conjugates the stresses and displacements in this series are real.

3.2. Other geometries

The above discussion presented a thorough analysis of the possible stress fields encountered in bonded structures in which the bonded strips meet at right angles. Other geometries, though, can exhibit drastically different stress fields. An excellent discussion of other geometries can be found in an article by Hein and Erdogan [8]. They consider bonded wedges of various opening angles and plot the order of the singularity for several geometries *versus* the ratio of the materials' elastic moduli. Because some of these cases produce no singularity, these results can, in theory, be used to eliminate singularities for a particular set of materials (by choosing appropriate geometries), or for a particular geometry (by appropriate material choice). It has not been shown experimentally that the singularities are harmful (given that they don't exist in nature), but the success of fracture mechanics, which is based on singular stress fields, indicates that singularities are indeed important and provide useful design information. The elimination of a singularity by design, though, won't eliminate stress concentrations at the edge, so one must be careful in assuming that this is advantageous. In any event, it provides an interesting problem for future research. Another interesting aspect of the work by Hein and Erdogan is that many of the singularities (for various geometries and material combinations) are oscillatory, i.e. the order of the singularity is complex. In this case the stress fields near the edge of the interface are of the form:

$$\sigma_{ij} \sim r^a \sin(b \ln r), \tag{54}$$

where a and b are the real and imaginary parts of the order of the singularity. One important example of this type of singularity occurs when an edge crack exists at the interface of two materials. In this case, the order of the singularity is given by:

$$\delta = 0.5 + b\sqrt{-1}, \tag{55}$$

where b ranges from 0 to 0.33, depending on the materials making up the bonded structure. The stresses, then, are of the form:

$$\sigma_{ij} \sim \sqrt{r} \sin(b \ln r). \tag{56}$$

One problem with this stress field is that the oscillations in the displacements along the surface of the crack lead to a predicted overlap of the crack surface, which is a physical impossibility. Comninou [9], though, considered the effects of interfacial pressure in the presence of such overlap, and found that the oscillations disappeared.

3.3. Particular solutions

As shown in the previous section, the solution for the near-edge stress fields in bonded structures can be described by the following equation:

$$[X]\{a\} = \{f\}, \tag{57}$$

where the matrix and vectors are defined in eq. (40). A solution to this equation exists if and only if the vector $\{f\}$ is orthogonal to all vector solutions of the equation [10]:

$$[X]^t\{a\} = 0. \tag{58}$$

If no solution exists, then the following solution for the Airy stress function is adopted:

$$\Phi = \frac{\partial}{\partial s}\{r^{-s}[a\sin s\theta + b\cos s\theta + c\sin(s+2)\theta + d\cos(s+2)\theta]\}, \quad (59)$$

which can also be written as

$$\Phi = r^{-s}\left(\frac{\partial}{\partial s} - \ln r\right)[a\sin s\theta + b\cos s\theta + c\sin(s+2)\theta + d\cos(s+2)\theta]. \quad (60)$$

This leads to a matrix equation of the form:

$$r^{-s}\left(\frac{\partial}{\partial s} - \ln r\right)[X]\{a\} = \{f\}, \quad (61)$$

which has a solution of the form:

$$[X]\{a\} = 0$$
$$\frac{\partial}{\partial s}([X]\{a\}) = \{f\}. \quad (62)$$

When the material properties and loadings are such that this type of solution holds, then a logarithmic stress singularity exists at the edge of the interface. The conditions for which such singularities are expected for thermal stresses in bonded structures will be mentioned in this section, but the analysis will not be carried further. Detailed analyses of logarithmic singularities in composites experiencing externally applied loads are discussed by Dempsey and Sinclair [11] and Zwiers et al. [12].

For bonded rectangles, the existence of a solution depends on the parameter $2k_1 - k_2$. If this parameter is zero, there is a solution vector to the associated homogeneous equation (eq. (58)), given by:

$$\{a\} = \{m'\ 0\ m'\ 0\ 4-m'\ 0\ 2\ 0\}. \quad (63)$$

This is not orthogonal to the forcing vector, so a logarithmic singularity is expected. For most materials, though, the only solution to equation 58 is:

$$\{a\} = \{0\ 1\ 0\ -1\ 0\ 1\ 0\ 0\}, \quad (64)$$

which is orthogonal to $\{f\}$. Hence, there is no logarithmic singularity and the particular solution to eq. (40) is:

$$a' = a'' = c' = c'' = 0 \quad (65)$$

and

$$b' = b'' = d' = d'' = \frac{2\mu'(n''\epsilon''_{in0} - n'\epsilon'_{in0})}{4(k-1) - k_2}. \quad (66)$$

This particular solution provides a mechanism for reducing thermal stresses in bonded structures. For components in a state of plane stress, the stresses can be reduced by matching the the thermal expansion coefficients of the two materials, but for plane strain, the quantity:

$$(1+\nu'')\alpha \quad -(1+\nu')\alpha' \quad (67)$$

should be minimized.

3.4. Solutions for finite bodies

The series solution for the stresses and displacements near the edge of the interface between bonded structures satisfies the equilibrium and compatibility conditions in the interior of two bonded structures, and it satisfies the boundary conditions on the free surface adjacent to the interface, but it does not satisfy the other boundary conditions. Solutions for finite bodies must account for this deficiency. The model shown in fig. 1 is used to explore the thermal and swelling stresses in bi-layered structures. Because the thermal and swelling fields and model geometry are symmetric about $x = l$, only half of the model must be considered, leaving only one singularity to accommodate. Since there is only one singularity, a single series solution, originating where the interface intersects the free surface, can be used to model the stresses throughout the body. The previously unknown coefficients must be determined such that the remaining boundary conditions are satisfied in some approximate manner. These additional stress boundary conditions are zero normal and shear stress on the surface parallel to the interface and zero shear stress along the symmetry line. The final boundary condition is that the displacements along the symmetry line in the axial (x) direction are uniform, which can be expressed by:

$$\frac{\partial u_x}{\partial y} = 0 \quad at \quad x = l. \quad (68)$$

This section will focus on the method for determining the coefficients in the series to satisfy these additional boundary conditions.

The method used here to determine the coefficients in the series is called, for lack of a better term, least squares collocation, following Wang and Choi [13]. This technique minimizes, in the least squares sense, the integral of the error in the boundary and symmetry conditions along the outside of the symmetric model. (A discussion of the merits of this method, relative to various others, can be found in a recent paper by the authors [6].) This process is begun by defining the following integral:

$$I = \int_{AB}\left(w_{y,y}\sigma_{yy}^2 + w_{x,y}\sigma_{xy}^2\right)\mathrm{d}x + \int_{BC}\left(w_{x,y}\sigma_x \quad \frac{\partial u}{\partial y} \quad 1\right)y,$$
$$+ \int_{CD}\left(w_{y,y}\sigma_{yy}^2 + w_{x,y}\sigma_{xy}^2\right)\mathrm{d}x, \quad (69)$$

(70)

which represents the integral of the errors in the series solution along the top, symmetry line and bottom, respectively. This residual integrand is given by the square of the difference between the prescribed boundary conditions and boundary values calculated from the approximate series solution. In most thermal and swelling stress problems the boundaries are traction-free, providing homogeneous boundary conditions. In this case the integrand is given by the stresses and displacements from the series solution alone. The normalization factors w_{ij} are used to non-dimensionalize the terms in this integral, but they also can be adjusted to emphasize a particular boundary condition on a particular side, in order to optimize the calculation of the unknown series coefficients. For this study, these normalization coefficients were taken to be the shear modulus of the associated strip. For a given number of terms in the series solution, the minimization of the residual integral gives the best available solution for the unknown series coefficients. Inserting the series representations for the stresses and displacements into this integral, including the particular solution, and taking the partial derivative with respect to each coefficient yields a linear system in the unknown coefficients. Because of the increase of the magnitude of each term in the series with increasing n, the resulting matrix is ill-conditioned. Hence, as before, higher precision is required for cases where extra terms are used in the series. This technique, then, can be used to study the stress fields in finite bonded structures. Applications of the method to fusion components follow in the next section.

4. Effects of swelling and irradiation creep

4.1. Nature of irradiation-induced strains

In the fusion environment, deformation of structural components in the radiation environment is generally described as inelastic. Inelastic strains are generated in solids which are subjected to a combination of external fields (e.g., applied stress, temperature, and irradiation). Such stresses may be of an elastic or non-elastic nature, depending on the material's behavior when the external field is removed. For example, moderate temperature excursions are usually associated with recoverable elastic strains, while the combination of an applied stress and high temperature usually produces nonrecoverable creep strains. In the event of irradiation at high temperatures, additional modes of deformation are introduced in the solid as a consequence of atomic displacements and subsequent microstructural rearrangements.

Neutron irradiation has been shown to result in two major deformation mechanisms, swelling and irradiation creep. While swelling is always accompanied by volume increases, which are sometimes substantial, irradiation creep is considered to be volume-conservative following the rules of plasticity. Irradiation strains, whether swelling or creep, are non-recoverable except for short transients on the order of point-defect mean lifetimes, so it is assumed that such strains are permanent and independent. Experimental and theoretical work have pointed out the interdependence of these two modes of deformation only through the mediation of the local stress. The stress dependence of swelling is generally weak, and that of irradiation creep is close to linear [14]. Since both irradiation creep and swelling are induced by a net point-defect flux to either dislocations or voids, they must, in some sense, be proportional to each other. This has been shown in many experiments.

In this paper both the swelling strain ϵ_s and the irradiation creep strain ϵ_{irr}^c are assumed to be linear functions of fluence, except for graphite in which densification usually occurs at the start of irradiation. Moreover, the swelling is assumed to be stress-independent and the creep strain rate is assumed to be linearly proportional to the applied stress. Nonlinear effects may indeed be important, but at this preliminary stage of analysis and with the unavailability of a large data base, little knowledge will be gained by investigating nonlinear effects. The irradiation swelling strain rate $\dot{\epsilon}_s$ will therefore be mostly constant (except for the densification of graphite), and the irradiation creep strain is assumed to obey the simple rule:

$$\frac{\partial \epsilon_{irr}^c}{\partial t} = B\phi\sigma, \tag{71}$$

where B is termed the creep compliance coefficient, ϕ is the accumulated neutron fluence (proportional to time), and σ is the local stress. It is interesting to note that the creep rate is linearly proportional to the stress in a manner reminiscent of viscous Newtonian fluids.

Viscoelastic materials undergo time-dependent deformations, which are generally described by an equation of the form [15]:

$$E\epsilon(t) = \sigma(t) + \int_0^t \kappa(t-\tau)\sigma(\tau)\,d\tau, \tag{72}$$

where $\kappa(t-\tau)$ is a material-dependent kernel representing the viscoelastic constitutive behavior and is the source of differences between creep and linear viscoelasticity. In many fusion applications, irradiation creep

rates dominate thermal creep rates, and the creep compliance, b, is nearly temperature independent. Because the form of creep strain relationship represented by eq (71) makes the kernel in eq. (72) constant, linear viscoelastic theory can be used to study the effects of swelling and irradiation creep on stress evolution in fusion devices.

In order to determine the stresses and strains in a viscoelastic body, the constitutive (stress–strain) relations must be modified to account for the time-dependent deformations. In general these relations are written:

$$P_1(D)s_{ij} = P_2(D)e_{ij} \tag{73}$$

and

$$P_3(D)\sigma_{ii} = P_4(D)(\epsilon_{ii} - 3\epsilon_{in}), \tag{74}$$

where

$$P_k(D) = \sum_{n=1}^{\infty} C_{kn}\frac{\partial^n}{\partial}. \tag{75}$$

A common solution method for these types of problems is to take the Laplace transform of the viscoelastic equations and compare the resulting set of equations to the steady-state formulation. Because the bulk behavior is often different from the shear behavior in viscoelastic materials, the stress–strain relations are usually written in terms of the stress and strain deviators S_{ij} and e_{ij}, defined as:

$$S_{ij} = \sigma_{ij} - \sigma_{ll}/3 \tag{76}$$

and

$$\epsilon_{ij} = \epsilon_{ij} - \epsilon_{ll}/3. \tag{77}$$

In terms of these quantities, the stress–strain relations are

$$S_{ij} = 2\mu e_{ij}, \tag{78}$$

and

$$\sigma_{ll} = 3\kappa\epsilon_{ll}, \tag{79}$$

where κ is the bulk modulus. Transforming eqs. (73) and (74) gives

$$\tilde{S}_{ij} = \frac{P_2(p)}{P_1(p)}\tilde{e}_{ij} \tag{80}$$

and

$$\tilde{\sigma}_{ii} = \frac{P_4(p)}{P_3(p)}\left(\tilde{\epsilon}_{ij} - 3\widetilde{\epsilon_{in}}\right), \tag{81}$$

where the Laplace transform of a function f is denoted by $\tilde{f}$. By comparing the elastic and viscoelastic constitutive equations, it is apparent that the solution of the viscoelastic problem in the Laplace domain is equivalent to the solution of the steady-state problem, with the elastic properties 2μ and 3κ replaced by $P_2(p)/P_1(p)$ and $P_4(p)/P_3(p)$, respectively. The time-dependent behavior of the viscoelastic problem is thus recovered by substituting the equivalent transformed properties into the steady-state, elastic solution and inverting the Laplace transform.

The primary difficulty in obtaining the inverse Laplace transform is that the eigenvalues s_k are not explicitly known because they are determined by solving a transcendental equation. The integral operator is unbounded, hence a small change in the transformed function can be lead to an arbitrarily large change in the desired time-dependent function. Therefore high precision is needed.

The method adopted in this work solves the Laplace transform as an integral equation, with $f(t)$ as the unknown function, using Gaussian quadrature. Other methods, such as those suggested by Miller and Guy [16] and Papoulis [17], may be used if the accuracy of the quadrature method is insufficient. The integral is approximated as a finite sum, using Nth order Gaussian quadrature. This can be evaluated for N arbitrary values of the Laplace parameter p, giving a linear system represented by

$$\tilde{f}(p_k) = \tfrac{1}{2}\sum_{i=0}^{N} w_i\left(\frac{1+\tau_i}{2}\right)^{p_k-1} g(\tau_i). \tag{82}$$

This gives a system of N equations for the N unknowns $g(\tau_i)$, which represent values of the unknown function $g(\tau)$ at discrete locations i. Also, the accuracy of the method depends on the order of the quadrature and on where the p_k's are chosen. Excellent agreement was found for exponential relaxation benchmark calculations with $p_k = k$ and $N = 15$. These values were adopted for Maxwell materials.

4.2. Viscoelastic creep models

Viscoelastic material behavior was recognized over a century ago [18]. Earlier modeling efforts considered various combinations of springs and dashpots to represent viscoelastic responses. In the Maxwell element model, the displacement rate/stress relationship is obtained by a serial combination of an elastic spring and a viscous dashpot. A Kelvin model, on the other hand, considers a parallel combination of the two elements. Various other representations of viscoelastic solids (e.g., the standard linear solid, the Burger model, and gener-

alized forms of the Maxwell or Kelvin models) are available as rearrangements of spring and dashpot elements. Only the Maxwell model will be used here.

In uniaxial tension/compression, the total strain, ϵ, which is composed of the elastic component, ϵ_e, and the inelastic component, ϵ_{in}, can be described by the constitutive relationship:

$$E\frac{\partial \epsilon}{\partial t} = \left(BE + \frac{\partial}{\partial t} \right)\sigma, \tag{83}$$

where the first term on the right-hand side represents an inelastic strain rate and the second term accounts for additive elastic strain rates. Extending eq. (83) to multiaxial deformation, one obtains:

$$\left(\frac{\partial}{\partial t} + \frac{1}{\tau_0} \right) S_{ij} = 2\mu \frac{\partial \epsilon_{ij}}{\partial t} \tag{84}$$

and

$$\sigma_{ii} = 3\kappa(\epsilon_{ii} - 3\epsilon_{in}), \tag{85}$$

where $1/\tau_0 = 2\mu B$. Now eqs. (84) and (85) can be rewritten in the general operator form of the viscoelastic constitutive equations (73) and (74), with the following definitions:

$$\begin{aligned} P_1(D) &= \frac{\partial}{\partial t} + \frac{1}{\tau_0}, \\ P_2(D) &= 2\mu \frac{\partial}{\partial t}, \\ P_3(D) &= 1, \\ P_4(D) &= \kappa. \end{aligned} \tag{86}$$

Taking the Laplace transform of the operators in equation 86 and substituting into equation 80 yields the following equivalencies between the elastic material properties and the viscoelastic "properties" in the Laplace domain:

$$2\mu \rightarrow \frac{2\mu p}{p + 1/\tau_0} \tag{87}$$

and

$$\kappa \rightarrow \kappa. \tag{88}$$

Using this equivalency, the elastic solution can be used to develop an equivalent solution in the Laplace domain by using the effective material properties:

$$\tilde{\mu} = \frac{\mu p}{p + 1/\tau_0} \tag{89}$$

and

$$\tilde{\nu} = \frac{1}{2}\left[\frac{3\kappa(p + 1/\tau_0) - 2p\mu}{3\kappa(p + 1/\tau_0) + p\mu} \right]. \tag{90}$$

4.3. Relaxation of inelastic stresses

For illustrative purposes, the thermal and swelling inelastic strains are represented by

$$\epsilon_{in} = C_0 + C_1 t, \tag{91}$$

where C_0 and C_1 are constants and t is time. The Laplace transform of this inelastic strain is given by:

$$\widetilde{\epsilon_{in}} = \frac{1}{p}\left(C_0 + \frac{C_1}{p} \right). \tag{92}$$

If the characteristic values of the matrix in eq. (40) are constants, the time dependence of the total solution depends only on the particular solution, which, for plane stress and a uniform temperature change can be written:

$$\widetilde{\sigma_{yy}} = \frac{\widetilde{\epsilon_{in}''} - \widetilde{\epsilon_{in}'}}{\tilde{\nu}''/\widetilde{E''} - \tilde{\nu}'/\tilde{E}'} \tag{93}$$

or, in terms of the Laplace parameter (for $\tau_0' = \tau_0'' = \tau_0$),

$$\widetilde{\sigma_{yy}} = 8\left(\frac{\mu'\mu''}{\mu' - \mu''} \right)\left[\frac{(C_0'' - C_0')}{p + 4/3\tau_0} + \frac{(C_1'' - C_1')}{p(p + 3/4\tau_0)} \right]. \tag{94}$$

Inversion of this equation gives the following time dependent behavior for the particular solution:

$$\begin{aligned} \sigma_{yy} = 8\left(\frac{\mu'\mu''}{\mu' - \mu''} \right)\big[&(C_0'' - C_0')\, e^{-4t/3\tau_0} \\ &+ \tfrac{4}{3}\tau_0(C_1'' - C_1')(1 - e^{-4t/3\tau_0}) \big]. \end{aligned} \tag{95}$$

Initial thermal stresses thus relax exponentially with time, and if a material swells at a constant rate, the swelling-induced stresses reach a steady-state value which is proportional to the difference between the swelling rates of the two materials and inversely proportional to the creep rate.

Contrary to crack problems, the order of the singularity of perfectly bonded viscoelastic materials depends on the material properties, as is shown by the characteristic values of the matrix equation (eq. (40)). Hence the order of the singularity will depend on the Laplace parameter p, due to the nature of the equivalency represented by eqs. (87) and (88). Therefore, in the case of perfectly bonded viscoelastic materials, the order of the singularity will be a function of time. For example, the transform of one of the material parameters, k, can be written:

$$\tilde{k} = \frac{\mu'}{\mu''}\left[\frac{p + 1/\tau_0''}{p + 1/\tau_0'} \right]. \tag{96}$$

As the Laplace parameter p ranges from 0 to ∞, k can

Table 2
Material properties used for fusion applications

	Graphite [20]	CuBe [23]	V–3Ti–1Si [23,24]	W–3Re [22]
Elastic modulus (GPa)	11	116	118	430
Expansion coefficient (K^{-1})	7.5×10^{-6}	17×10^{-6}	10×10^{-6}	4.8×10^{-6}
Poisson's ratio	0.11	0.34	0.36	0.36
Thermal conductivity (W/m K)	110	135	28	67
Melting point (°C)	–	1100	1900	3400

take on virtually any value, depending on the creep constants of the two materials. This can be shown using the final value theorem of the Laplace transform, which indicates that as t approaches infinite, k approaches a limiting value given by

$$k_\infty = B''/B'. \tag{97}$$

Hence, the initial value of this parameter depends only on the elastic properties (μ'/μ'') and the final value depends only on the creep rates, leading to the potential for arbitrary variation of k over the component lifetime. In addition, the dramatic impact that this parameter has on the order of the singularity in bonded structures indicates that, over time, the order can vary anywhere in the range $0 < s_1 < 0.41$.

4.4. Illustrative fusion applications

As representative examples of two material combinations for duplex fusion components, two substrate materials (copper and vanadium) and two surface materials (graphite and tungsten) are chosen to study the impact of interface singularities in fusion components. Copper is picked for its high thermal conductivity and vanadium for its swelling resistance and relatively good high-temperature strength. Because graphite has a relatively short lifetime (due to radiation damage), it is not a viable candidate for commercial fusion reactors, but it can be used for near-term machines because the neutron fluence at the end-of-life is relatively small. Therefore, graphite on copper is chosen to represent duplex components for near-term devices, and the tungsten on vanadium duplex is chosen to represent commercial fusion applications.

Several alloys are possible for these two duplex structures. The choice is generally governed by the alloy's radiation response and physical properties. Here a Cu–Be alloy is chosen because of its low swelling rate, consistent with the INTOR design [19]. A highly isotropic graphite (POCO Graphite Corporation's grade AXF-5Q, for example) is used as a surface material because of its low swelling and high strength [20]. For vanadium, a V–3Ti–1Si alloy is chosen as the substrate material for the commercial reactor application primarily because of its reduced susceptibility to helium embrittlement induced by radiation damage [21]. Tungsten alloy choices are more limited than those for vanadium or copper because a significant shift in the ductile-to-brittle transition temperature (DBTT) is caused by neutron irradiation of pure tungsten. However, alloying additions of rhenium have shown a beneficial effect on the ductility of tungsten [22]. Therefore, the properties of a W–3Re alloy [22] will be used for this analysis. The unirradiated material properties used in this study are given in table 2.

4.5. A near-term application

Pure copper is prone to high swelling rates, with measured values of up to 7% after only 15 dpa [25]. The addition of beryllium to copper, however, reduces the propensity to swelling. At 450 °C, Cu–Be was found to densify up to 0.66% at 16 dpa [26]. The thermal conductivity of Cu–Be is not expected to change by low-dose irradiation [26].

Graphite volume change by irradiation is caused by the growth of the hexagonal crystals perpendicular to their basal planes, and the crystal shrinkage within this plane. The initial stage of irradiation is accompanied by densification because the irradiation growth is absorbed in internal fabrication porosities, while the transverse shrinkage results in overall densification. When all fabrication porosity is filled the graphite tends to swell rapidly as illustrated in fig. 5. The end of life is reached when accelerated swelling begins [27], causing lifetimes shorter than one year. One other important aspect of graphite behavior is the degradation of the thermal conductivity with irradiation.

The following assumptions are made in the graphite/Cu–Be duplex study:

1. Negligible effects of irradiation on the degradation of the elastic properties (this is probably not valid

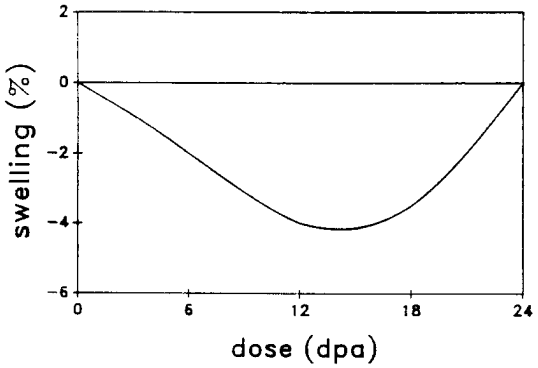

Fig. 5. Swelling of graphite [23].

for most graphites, but time-dependent moduli cannot be incorporated in the present model, due to computational difficulties).

2. There is no irradiation creep in either material. (Again, this is not valid for graphite, but the present example is intended to show the effects of swelling, without creep. The following example – vanadium/tungsten – will show the effects of creep.)
3. An initial 0.2%/dpa densification rate for Cu–Be (here it is assumed that the subsequent swelling of the Cu–Be does not begin until after the end-of-life for the graphite).
4. Nonlinear graphite densification as shown in fig. 5.
5. A linear decrease in graphite conductivity to one quarter of the unirradiated value by the end of life.
6. A braze temperature of 800 °C [28].

This list shows that the present model is incapable of representing the true behavior of graphite, due to it's time dependent elastic modulus and nonlinear swelling curve. Hence, the time-dependent results shown below are representative of an analysis of creep-free materials with constant properties. A later example will include creep effects to show their impact on the time dependent singularities.

Table 3
Boundary-layer stress intensity factors for a graphite layer on a Cu–Be substrate

Intensity factor (MPa $m^{0.07}$)	Fabrication	Startup
$K_{rr'}$	136	74
$K_{rr''}$	−49	−27
$K_{r\theta}$	−52	−28
$K_{\theta\theta}$	−764	−412

The Cu–Be/graphite component is modeled by assuming that it consists of a 5-mm-thick graphite tile on a 5-mm-thick Cu–Be substrate, each 40 mm long. Plane strain conditions are assumed. This idealization is not intended to be for the actual divertor or limiter, but it should represent the influence of various loadings on the crack-free stress intensities near the edge of the interface in such components. The peak, full-power heat flux is taken to be 5 MW/m^2. The order of the stress singularity for this duplex is 0.07.

The tortuous history that a fusion component experiences begins with its fabrication. For a brazed part, fabrication takes place at high temperatures, leading to differential contraction during cooldown if the constituents have different thermal expansion coefficients. As the component is cooled from its brazing temperature, the filler metal will freeze at some points, thus locking the interface and causing thermal stresses as the part cools further. For the graphite–copper components described, this lockup is assumed to occur at 700 °C, a difference of 100 °C from the brazing temperature. The stresses caused by this process can be calculated from the model developed for this paper by considering a uniform temperature change of −670 °C, assuming that room temperature is 30 °C. This leads to the boundary-layer stress intensity factors as shown in table 3. The azimuthal stress intensity $K_{\theta\theta}$ is negative here, indicating that the tear-away stress (the stress normal to the interface) at the edge of the interface is compressive, thus, perhaps, preventing delamination. Also, the magnitude of this boundary-layer stress intensity is greater than any of the other four. This is insignificant, though, because the ratios of the different stress intensities depend only on the materials involved. Hence, this disparity would be accounted for automatically by any measurements of the critical boundary-layer stress-intensity factors. Experiments must be conducted to determine whether these stress intensities are sufficiently high to cause crack initiation or failure.

The startup of a fusion machine consists of several steps. First, the entire device is heated fairly uniformly to a temperature near the operating temperature for full-power operation. This brings the component nearer to the brazing temperature so, assuming that the residual stresses resulting from the fabrication process have not relaxed, this initial heating will actually reduce the stresses in the component. In this case, heating to an equilibrium temperature of 300 °C will reduce the residual stresses by more than 50% (actually by the ratio 400/670).

After bringing the reactor to a uniform temperature near the operating temperature, the reactor power is

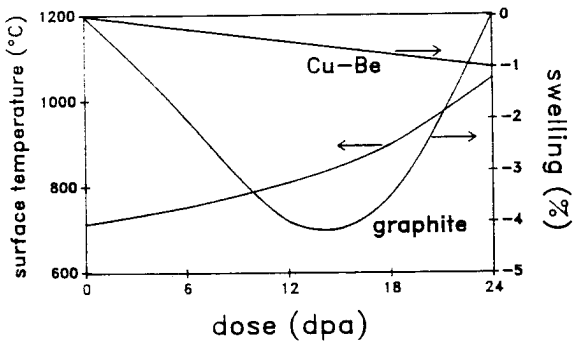

Fig. 6. Surface temperature and swelling of both materials for the copper–graphite component.

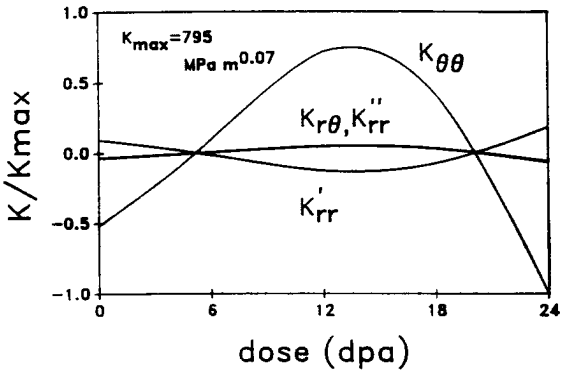

Fig. 7. Boundary-layer stress intensities in copper–graphite component during full-power operation.

ramped up to full power, pausing at different levels for any required testing. When the power is initiated, the associated heat flux sets up thermal gradients in the plasma-facing components, thus introducing an additional source of stresses. For a copper surface temperature of 300 °C, the 5-MW/m^2 heat flux leads to an interface temperature T_i of 485 °C and a graphite surface temperature T_s of 715 °C. This gradient, on top of the stresses remaining from the fabrication and uniform heating, leads to the stress intensity factors shown in table 3. The tear-away stress is compressive and is dominated by the residual fabrication stresses. Fig. 6 shows several results: (1) The decreasing graphite thermal conductivity leads to an increasing thermal gradient in the top layer, so the surface temperature increases with the dose. (2) The surface temperature and swelling are shown as a function of dose. (3) The surface temperature goes from a low of 715 °C to a high of 1053 °C, but the interface temperature doesn't change because the thermal conductivity of the copper is not affected by the damage. (4) The percent volume change caused by the damage shows that the graphite initially densifies much quicker than the copper. After about 15 dpa though, the graphite volume begins to increase while the Cu–Be alloy continues to densify. The graphite is assumed to fail at about 24 dpa, where its density returns to its original value.

Because the damage behavior of the graphite is highly nonlinear, the resulting boundary-layer stress intensities vary significantly as a function of the radiation dose. This is shown in fig. 7, which plots the four stress intensities as a function of dose. The largest of the four, $K_{\theta\theta}$, begins at about half its peak value, and changes sign at about 5 dpa and again at about 19 dpa. This stress intensity reaches its peak magnitude at the end-of-life dose of 24 dpa. Failure could occur before this time if the allowable stress intensity is degraded by the damage, or if tensile tear-away stresses are more severe than compressive values of equal magnitude.

The time-dependent boundary-layer stress intensity $K_{\theta\theta}$ for the copper-graphite component is shown in fig. 8, which includes the fabrication and startup responses. During the cooldown from the brazing temperature, the copper shrinks faster than the graphite and the resulting stress intensity is negative. The subsequent uniform heating prior to startup reduces the magnitude of this residual stress intensity as shown, while the heat fluxes associated with the onset of power cause a slight increase. As the radiation damage begins, the graphite densifies faster than the copper alloy. Thus the magnitude of the stress intensity is reduced because of slower graphite shrinkage during cooldown from the braze temperature. This phenomenon causes the stress intensity to become positive until the graphite begins to expand again at around 15 dpa. This leads to an end-

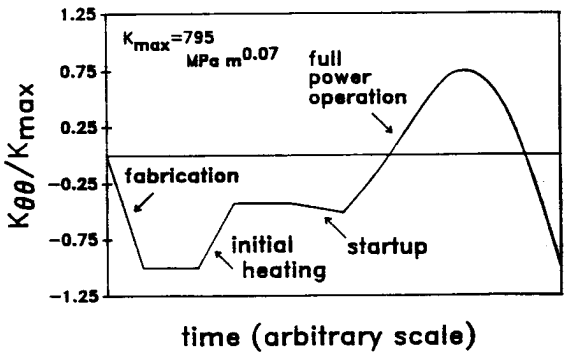

Fig. 8. Boundary-layer stress intensities in copper–graphite component.

of-life stress intensity of about the same value as the initial residual stress intensity resulting from fabrication.

4.6. Commercial fusion application

For the analysis of the tungsten–vanadium duplex, the model consists of a 2-mm-thick tungsten layer on a 1.5-mm-thick vanadium strip. The length is taken to be 10 mm and only the plane strain state is considered. The heat flux is again chosen to be 5 MW/m^2. For this duplex, the calculated order of singularity is 0.12, which is slightly stronger than that for the graphite-copper combination. Given the assumed grazing temperature of 1000 °C and an assumed lock-up temperature of 900 °C, the calculated fabrication boundary-layer stress intensities are shown in table 4. In a startup scenario, an initial uniform temperature of 450 °C is assumed, which was found to reduce the residual stresses by more than half. The onset of reactor power operation at 5 MW/m^2 surface heating produces an interface temperature of 718 °C and a peak tungsten surface temperature of 867 °C. The calculated average temperatures of 793 °C and 584 °C in the tungsten and vanadium, respectively, are important because they determine the relative swelling rate of the two materials. The residual stresses, combined with the thermal gradients at the onset of reactor operation lead to the stress intensities given in table 4.

The swelling rate of pure vanadium can be significant (~0.05%/dpa). However, alloying, particularly with titanium, can result in a dramatic decrease in this rate. Braski [21] has measured the swelling rate in V–3Ti–1Si to be about 0.002%/dpa at 420 °C with an implanted helium level of 82 appm. The Blanket Comparison and Selection Study (BCSS) [29] estimates that swelling rates of this order will occur until about 175 dpa, after which the swelling rate will increase to about 1%/dpa. Relevant data on the temperature dependence for the swelling of vanadium and tungsten is very scarce. Therefore, it is assumed that the temperature

Table 4
Unirradiated stress intensity factors for the V–W duplex

Intensity factor (MPa m$^{0.12}$)	Fabrication	Startup
$K_{rr'}$	180	51
$K_{rr''}$	−331	−110
$K_{r\theta}$	−131	−38
$K_{\theta\theta}$	−664	−189

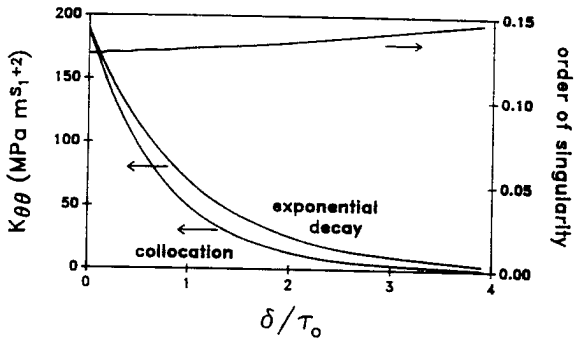

Fig. 9. Dose dependence of the order of the singularity and the boundary-layer stress intensity in a tungsten/vanadium duplex, without swelling.

dependence of these two alloy systems is similar to the refractory alloy, TZM, at the same homologous temperature. It will further be assumed that the irradiation creep rate of both V–3Ti–1Si with W–Re alloys is identical to that of titanium. An average value of the creep compliance, B, of 1.5×10^{-27} MPa^{-1} (n/cm^2)$^{-1}$ will be used in this study. This value is based on Nygren's creep measurements on Ti [30]. This is equivalent to a creep rate of 2×10^{-6} MPa^{-1} dpa^{-1}. The sensitivity of the results to this value will be studied by varying the creep rates of both vanadium and tungsten. The physical and elastic properties of both materials are also assumed to be unchanged under irradiation.

The analysis of the tungsten-vanadium duplex under irradiation is complicated by the occurrence of irradiation creep in both materials. This deformation relaxes the thermal stresses and reduces the effects of the swelling. As mentioned earlier, the swelling of both materials is expected to be quite small so the initial analysis consists of relaxation of the initial stresses. Assuming identical creep constants $\tau_0' = \tau_0'' = 1.3$ dpa, the relaxation is shown in fig. 9 The azimuthal stress intensity $K_{\theta\theta}$ is shown to relax to zero within just a few dpa. Considering that the expected lifetime of a typical reactor component is over 100 dpa, this relaxation takes place very early in the life of the component, and the stresses will be essentially zero as long as the reactor power continues. Of course, a portion of these stresses will be recovered (as residual stresses) when the power is turned off. Fig. 9 shows a companion curve with an exponential decay of the initial stress intensity. The relaxation for a Maxwell material is exponential so, under most conditions, the decay of an initial thermal stress would also be exponential. However, for a bonded material, the order of singularity also changes so the

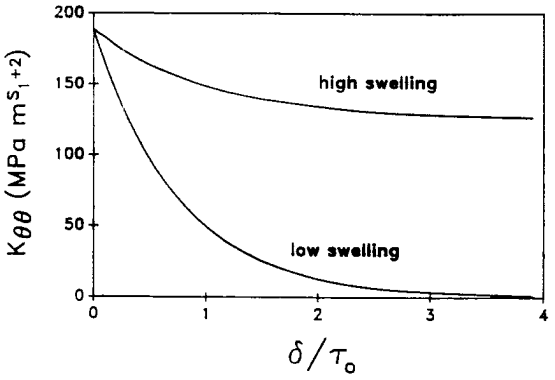

Fig. 10. Relaxation of boundary-layer stress intensity with and without swelling.

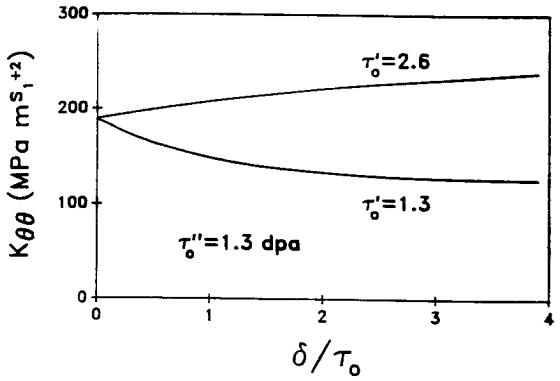

Fig. 11. Dose dependence of the boundary-layer stress intensity for two different vanadium creep constants.

decay is altered. It is also shown that the order of singularity actually increases slightly, causing a faster than expected decay of the stress intensity. The implications of this behavior on the initiation of failure are unclear.

If the assumed swelling behaviors of the materials in this component are in error, there may be a significant swelling in one or both of the layers. To study this, the tungsten will be assumed to swell at the rate of 0.2%/dpa. Because the material is continuously expanding as the radiation damage occurs, the stresses in the component reach a steady-state level where the swelling rate is balanced by the creep relaxation rate. This level is determined by the two rates, and by the amount of self-constraint associated with the structure. This phenomenon is shown in fig. 10, where the boundary-layer stress intensity relaxes to a steady value of around 106 MPa m^{s_1+2} within just a few time constants. The fact that the stress intensity decreases, even in the high swelling case, is a result of several factors and is not a general result. If the swelling rate was higher, all other factors being equal, then the stress intensity could increase despite the creep relaxation. The relaxation time would scale with the time constant τ_0 and the steady-state stress intensity would be proportional to the relaxation constant. One complication arises, though, when one creep rate changes relative to the other. In this case the scaling arguments, which are possible if both rates changes, are not valid. Fig. 11 shows the dose dependence of the boundary layer stress intensity for two different creep rates. When the creep constant, τ_0, is identical for both materials, the stress intensity is shown to relax to a steady-state value of about 106 MPa m^{s_1+1}. When the creep constant in the vanadium is increased to 2.6 dpa (indicating a slower creep rate), the steady-state stress intensity increases to about 240 MPa m^{s_1+2}. As a companion to fig. 11, fig. 12 shows the time dependence of the order of the singularity. Whereas the steady-state stress intensity increased with the increased creep constant, the end-of-life order of singularity decreases. The change, though, is quite small over the life of the component.

The effects of changing a single creep rate are again illustrated in fig. 13, showing how both the steady-state stress intensity and the order of singularity vary with the vanadium creep constant for a fixed tungsten creep rate. The steady-state stress intensity is seen to increase as the creep in the vanadium slows, while the order of singularity decreases. The increase in the stress intensity is quite strong, but if τ_0' were increased sufficiently, the order would go to zero and the singularity would disappear. This occurs because as the creep in the vanadium slows, it becomes effectively stiff, relative to the tungsten. Because the tungsten was originally stiffer than the

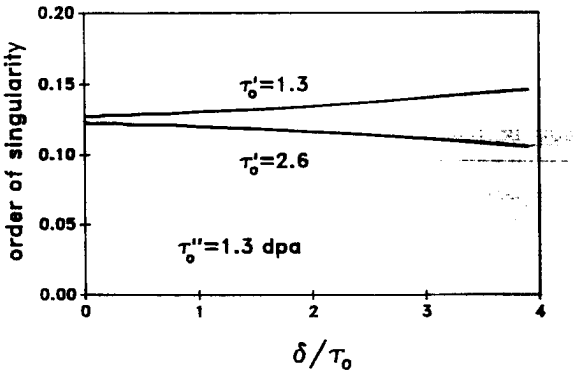

Fig. 12. Dose dependence of the order of the singularity for two different vanadium creep constants.

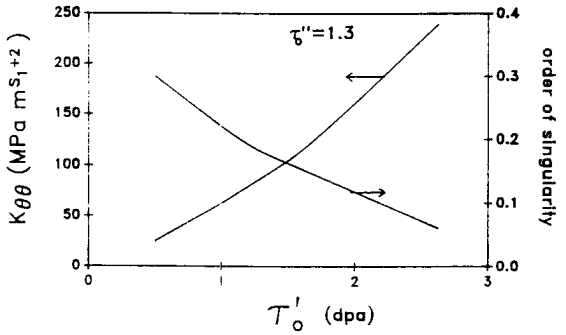

Fig. 13. Steady-state stress intensity and order of singularity for varying vanadium creep rate.

vanadium, the effective stiffening of the vanadium brings the ratio of the stiffnesses closer, thus eliminating the singularity.

Acknowledgements

This research was performed under appointment to the Magnetic Fusion Energy Technology Fellowship Program administered at Oak Ridge Associated Universities for the United States Department of Energy. Financial support for Professor Ghoniem was provided by the Office of Fusion Energy, US Department of Energy, Grant # DE-FG03-86ER52126.

References

[1] S. Timoshenko, J. Strain Anal. 11 (1925) 233.
[2] B. Boley and J. Weiner, Theory of Thermal Stresses (Wiley, New York, 1960) pp. 429–431.
[3] H.E. Williams, J. Thermal Stresses 6 (1983) 231.
[4] D. Chen, S. Cheng and T. Gerhardt, J. Thermal Stresses 5 (1982) 67–84.
[5] M. Goland and E. Reissner, J. Appl. Mech. 1 (1944) A17–A27.
[6] J. Blanchard and N. Ghoniem, to be published in J. Thermal Stresses.
[7] D. Muller, Math. Tables and Other Aids to Computer 10 (1956) 208.
[8] V.L. Hein and F. Erdogan, Int. J. Fracture Mech. 7 (1971) 317.
[9] M. Comninou, J. Appl. Mech. 44 (1977) 631–636.
[10] F. Hildebrand, Methods of Applied Mathematics (Prentice–Hall, New Jersey, 1965).
[11] J.P. Dempsey and G.B. Sinclair, J. Elasticity 9 (1979) 373.
[12] R. Zwiers, T. Ting and R. Spilker, J. Appl. Mech. 49 (1982) 561.
[13] S.S. Wang and I. Choi, J. Appl. Mech. 49 (1982) 549.
[14] J. Gittus, Creep, Viscoelasticity and Creep Fracture in Solids (Applied Science, Essex, England, 1975).
[15] Y.N. Rabotnov, Creep Problems in Structural Members (Elsevier, New York, 1969) p. 122.
[16] M.K. Miller and W.T. Guy, Jr., SIAM J. Numer. Anal. 3 (1966) 624.
[17] A. Papoulis, Quart. Appl. Math. 14 (1957) 405.
[18] D.R. Axelrad, Adv. Mol. Relaxation Processes 2 (1970) 41–68.
[19] R.F. Mattas et al., Fusion Technol. 10 (1986) 364.
[20] G. Engle and B. Kelly, J. Nucl. Mater. 122 & 123 (1984) 122.
[21] D. Braski, J. Nucl. Mater. 141–143 (1986) 1125.
[22] Corporate Publication, Metallwerk Plansee GmbH, A-6600 Reutte.
[23] R. Mattas, D. Smith and M. Abdou, J. Nucl. Mater. 122 & 123 (1984) 66.
[24] D. Smith, B. Loomis and D. Diercks, J. Nuc. Mater. 135 (1985) 125.
[25] R. Livak, T. Zocco and J. Kennedy, ADIP Semi-Annual Progress Report DOE/ER-0045/14 (1985) 152–160.
[26] H. Brager, H. Heinisch and F. Garner, ADIP Semi-Annual Progress Report DOE/ER-0045/13 (1984) p. 183–187.
[27] W. Green, D. Smith and B. Kelly, J. Nucl. Mater. 122 & 123 (1984) 14.
[28] M. Schwartz, Brazing (ASM International, Metals Park, Ohio, 1987).
[29] D. Smith et al., ANL/FPP-84-1 3 (1984) 7-123.
[30] R. Nygren, J. Nucl. Mater. 85 & 86 (1979) 861.